

ELECTRONIC SUPPLEMENTARY INFORMATION

Controlling the non-linear emission of upconversion nanoparticles to enhance super-resolution imaging performance

Simone De Camillis ^{*,a}, Peng Ren ^{a,b}, Yueying Cao ^{a,c}, Martin Plöschner ^{a,d}, Denitza Denkova ^{a,e},
Xianlin Zheng ^a, Yiqing Lu ^{*,a,b}, James A. Piper ^a

^aARC Centre of excellence for Nanoscale Biophotonics (CNBP), Department of Physics and Astronomy, Macquarie University, NSW 2109, Australia.

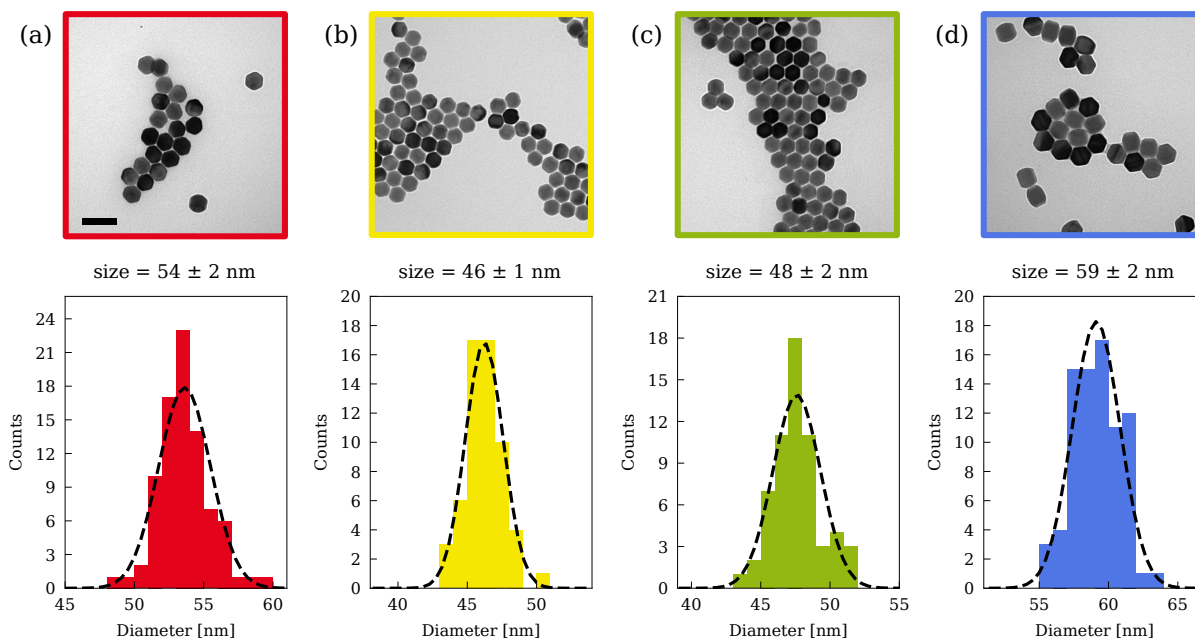
^bCNBP, School of Engineering and Physics, Macquarie University, NSW 2109, Australia.

^cCNBP, Department of Molecular Sciences, Macquarie University, NSW 2109, Australia.

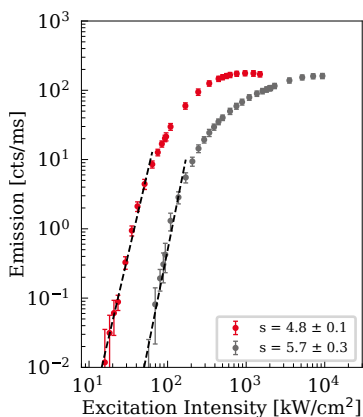
^dSchool of Information Technology and Electrical Engineering, The University of Queensland, QLD 4072, Australia.

^eInstitute for BioEngineering of Catalonia (IBEC), 08028 Barcelona, Spain.

*Corresponding authors: simone.decamillis@mq.edu.au, yiqing.lu@mq.edu.au

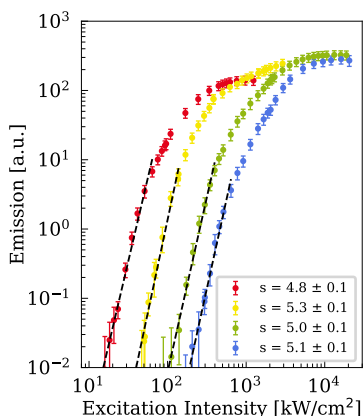


Supplementary Figure 1: **TEM images and size distribution of the core-only nanoparticle samples**, $\text{NaYb}_x\text{Tm}_{1-x}\text{F}_4$ with $x = 0.92, 0.88, 0.84, 0.8$, represented in (a), (b), (c), and (d), respectively. The sample size is estimated by the Gaussian best-fit of the diameter distribution. Bar scale: 100 nm.

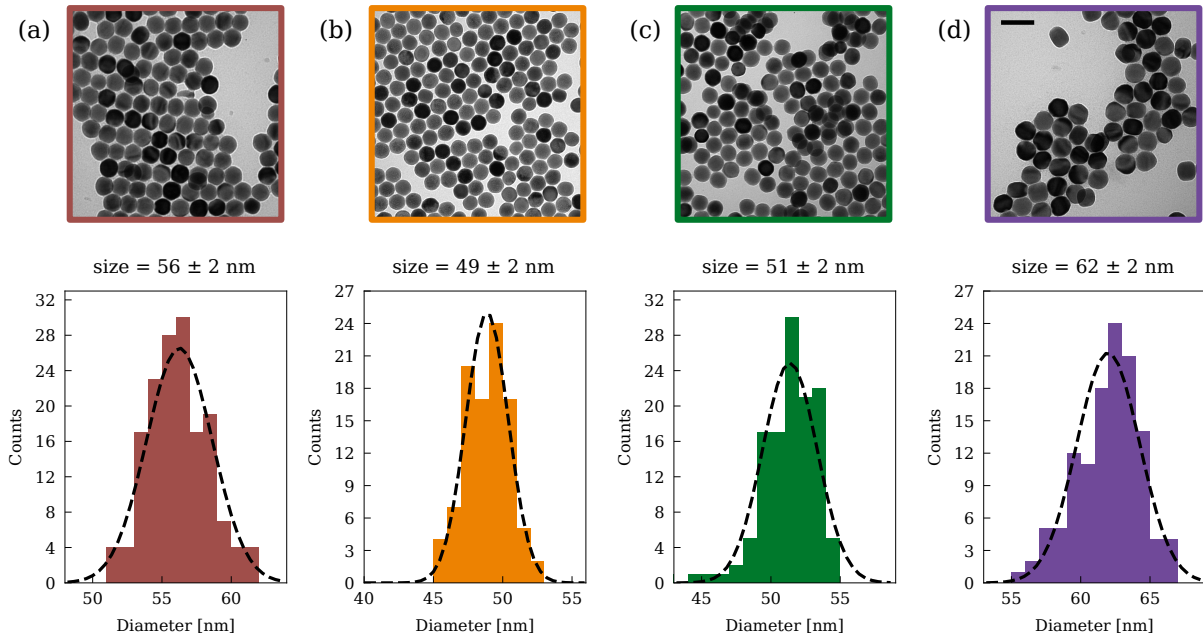


Supplementary Figure 2: **Comparison between the fully Yb-based nanoparticles and the common Y-based ones at fixed Tm doping concentration.** The sample $\text{NaYb}_{0.92}\text{Tm}_{0.08}\text{F}_4$ is represented in red, while the sample $\text{NaY}_{0.72}\text{F}_4:\text{Yb}_{0.20}\text{Tm}_{0.08}$ (two-step growth, average size of 45 nm)¹ in grey. With the same level of Tm concentration, we observe that the intensity threshold for sample 92/8 is more than three times smaller than for the sample 20/8, $I_{\text{th}} = 15$ and 50 kW cm^{-2} , respectively.

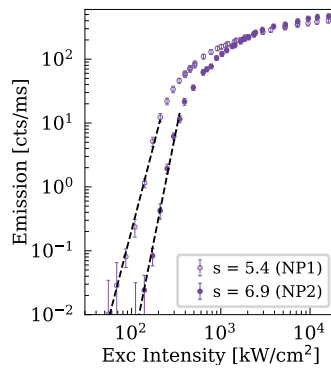
¹D. Denkova *et al.*, “3D sub-diffraction imaging in a conventional confocal configuration by exploiting super-linear emitters”, *Nature Communication* **10**, 1 (2019).



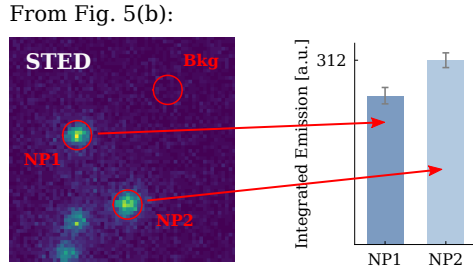
Supplementary Figure 3: **Volume-normalised emission curves as function of the excitation intensity.** The samples $\text{NaYb}_x\text{Tm}_{1-x}\text{F}_4$ with $x = 0.92, 0.88, 0.84, 0.8$ are represented in red, yellow, green, and blue, respectively. Volume normalisation is performed to qualitatively compare the UCNPs saturation levels, suggesting a slight increase of the saturation yield with increasing concentration of the Tm ions. The normalisation also shows corresponding values of the emission slope (best fit represented in dashed line and reported in the legend) with respect to the original data. A quantitative analysis is limited by approximations on the nanoparticle composition (i.e. uniform distribution of the doping ions, shape of the nanoparticles) required for the curve normalisation.



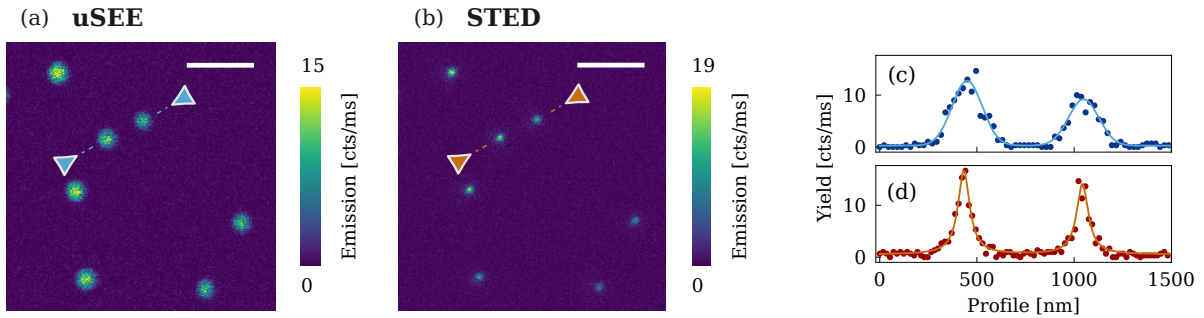
Supplementary Figure 4: **TEM images and size distribution of core-shell nanoparticle samples, $\text{NaYb}_x\text{Tm}_{1-x}\text{F}_4@ \text{NaYF}_4$ with $x = 0.92, 0.88, 0.84, 0.8$, represented in (a), (b), (c), and (d), respectively.** An average shell thickness of 1.5 nm can be estimated by comparing the size distribution of the core-only and core-shell nanoparticles. Bar scale: 100 nm.



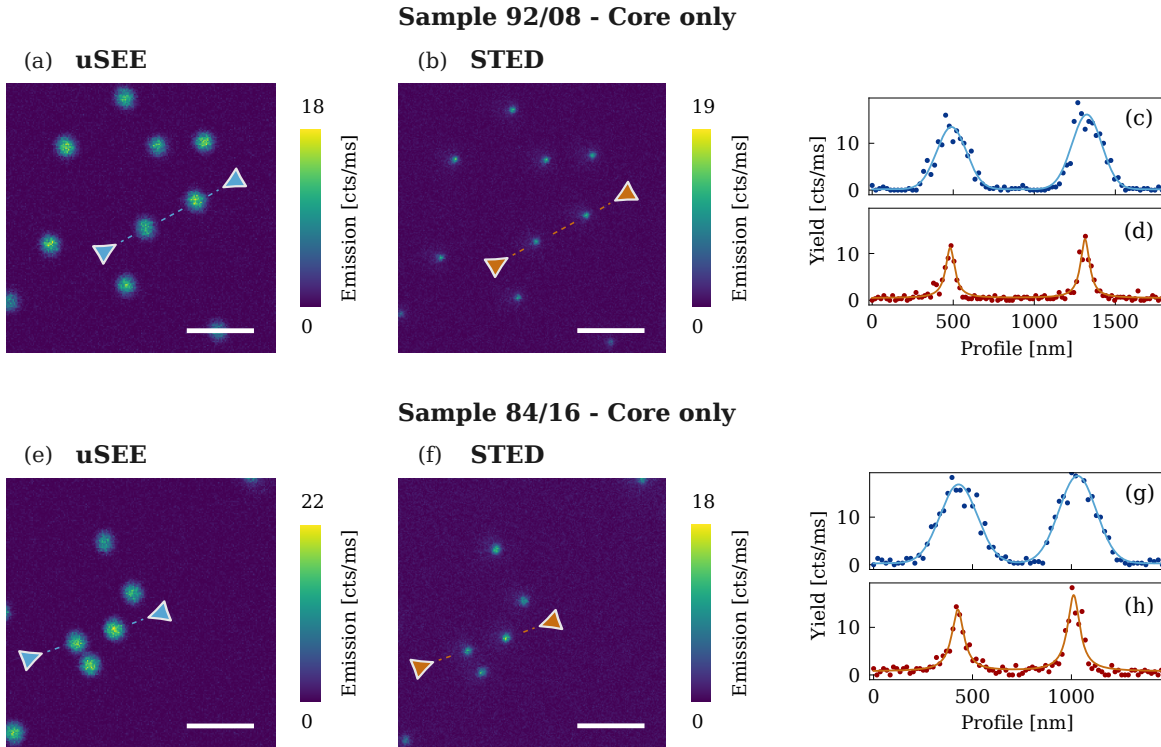
Supplementary Figure 5: **Deviations in the emission curve between nanoparticles of the core-shell sample 80/20, due to the inhomogeneity in the shell thickness.** These variations are particularly pronounced for nanoparticles with low Yb/Tm concentration ratio. Here we reported the largest variation in emission curve between two particles of the same sample. Particle 1 and 2 show an excitation threshold of $I_{\text{th}} = 57$ and 121 kW cm^{-2} , respectively.



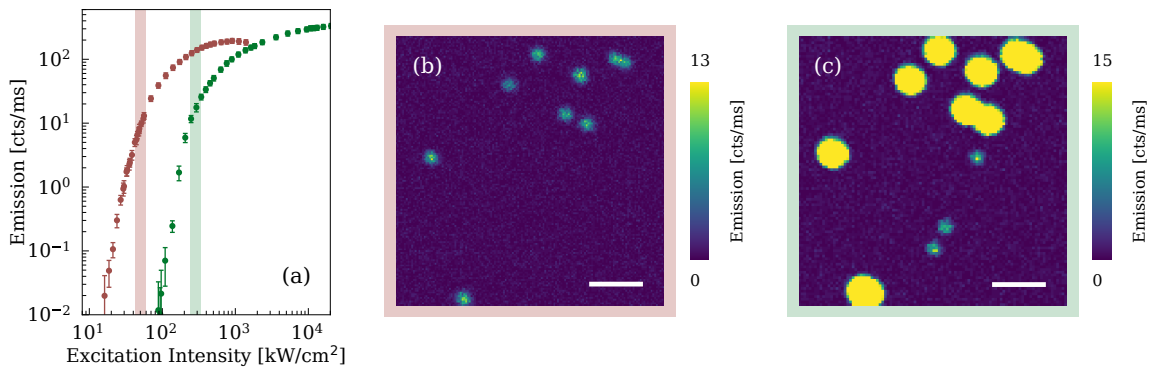
Supplementary Figure 6: **Integrated emission of nanoparticles to verify absolute brightness with respect to the uSEE images.** The relative heights of the emission peaks in STED mode (Figures 5(b,d)) compared to uSEE mode (Figures 5(a,c)) are affected by the limited spatial sampling of the NP profile and the image noise. We performed a simple check by integrating their emission distributions, since the integration is affected less by pixel alignment. The integrated amplitude with background subtraction shows a comparable peak ratio with the line profile in uSEE mode.



Supplementary Figure 7: **Super-resolution imaging of core-shell nanoparticles with Yb/Tm concentration ratio $\eta = 84/16$, $\text{NaYb}_{0.84}\text{Tm}_{0.16}\text{F}_4@ \text{NaYF}_4$.** (a) Confocal image of the UCNPs by means of the uSEE technique (203 kW cm^{-2}). (b) Same confocal imaging scan as in (a) performed with the STED technique (excitation and depletion intensities equal to 0.245 and 8.6 MW cm^{-2} respectively). Dwell time: 3 ms . Scale bar: $1 \mu\text{m}$. (c-d) Line profiles to evaluate super-resolution performance, with best resolution of $183 \pm 13 \text{ nm}$ for uSEE and $72 \pm 6 \text{ nm}$ for STED, respectively.



Supplementary Figure 8: **Super-resolution imaging of core-only nanoparticles with Yb/Tm concentration ratio 92/8 ($\text{NaYb}_{0.92}\text{Tm}_{0.08}\text{F}_4$) and 84/16 ($\text{NaYb}_{0.84}\text{Tm}_{0.16}\text{F}_4$).** At similar signal and resolution performance, the core-only samples require higher excitation powers, at least 30% higher for sample 92/8 and at least 55% for sample 84/16. Moreover, we do observe some deterioration in resolution for the core-only nanoparticles in uSEE mode due to the reduced emission slope. (a,e) Confocal images of the UCNP's by means of the uSEE technique (excitation intensity of 63 and 422 kW cm^{-2} , for sample 92/8 and sample 84/16 respectively). (b,f) Same confocal imaging scans as in (a,e) performed with the STED technique (excitation and depletion intensities equal to 0.067 and 5.4 MW cm^{-2} for the sample 92/8, 0.423 and 13.3 MW cm^{-2} for the sample 84/16). Dwell time: 3 ms. Scale bar: 1 μm . (c,d) Line profiles to evaluate super-resolution performance of sample 92/8, with best resolution of 215 ± 14 nm for uSEE and 67 ± 7 nm for STED, respectively. (g,h) Line profiles to evaluate super-resolution performance of sample 84/16, with best resolution of 222 ± 11 nm for uSEE and 74 ± 8 nm for STED, respectively.



Supplementary Figure 9: **uSEE multiplexed imaging, distinguishing the two core-shell UCNP's with $\eta = 92/8$ and 84/16 mixed together,** represented in dark red and dark green, respectively. (a) Single-nanoparticle 455-nm emission curve of each sample. (b) Excitation intensity of 50 kW cm^{-2} . (c) Excitation intensity of 207 kW cm^{-2} . Dwell time: 3 ms. Scale bar: 1 μm .

Supplementary Note 1: Simulation of the effects of the core-shell structure on the excitation-emission curve

Coating UNCPs with a thin inert shell significantly reduces surface quenching, boosting the excited-state populations of the emitter ions. This mechanism can effectively enhance the emission slope and potentially improve the emission yield of the nanoparticle at lower excitation powers. To confirm this hypothesis, we built a simplified energy level diagram, illustrated in Supplementary Figure 10(a), which involves two energy levels associated with the sensitiser ions (represented as n_1 and n_2 , respectively) and three levels related to the emitter ions (represented as n_3 , n_4 , and n_5 , respectively), as well as two levels of the surface defects. The following assumptions are applied: (a) the excitation photons are absorbed by the sensitiser ions only, (b) energy transfer occurs between the excited population of the sensitiser ions, the surface defects and both the ground and the intermediate levels of the emitters, (c) a cross-relaxation mechanism takes place in the emitter ions between the ground state and the upper-excited levels, (d) the non-radiative relaxation of the excited-state surface defects is very rapid compared to other pathways, and (e) other non-radiative relaxation pathways are ignored. Hence, the following rate equations can be obtained:

$$\frac{dn_1}{dt} = -Pn_1 + W_s n_2 + c_1 n_2 n_3 + c_2 n_2 n_4 + k_q n_2 \quad (1)$$

$$\frac{dn_2}{dt} = Pn_1 - W_s n_2 - c_1 n_2 n_3 - c_2 n_2 n_4 - k_q n_2 \quad (2)$$

$$\frac{dn_3}{dt} = -c_1 n_2 n_3 + W_4 n_4 + b W_5 n_5 - k_c n_3 n_5 \quad (3)$$

$$\frac{dn_4}{dt} = c_1 n_2 n_3 - c_2 n_2 n_4 - W_4 n_4 + (1 - b) W_5 n_5 + 2k_c n_3 n_5 \quad (4)$$

$$\frac{dn_5}{dt} = c_2 n_2 n_4 - W_5 n_5 - k_c n_3 n_5 \quad (5)$$

$$n_1 + n_2 = 1 \quad (6)$$

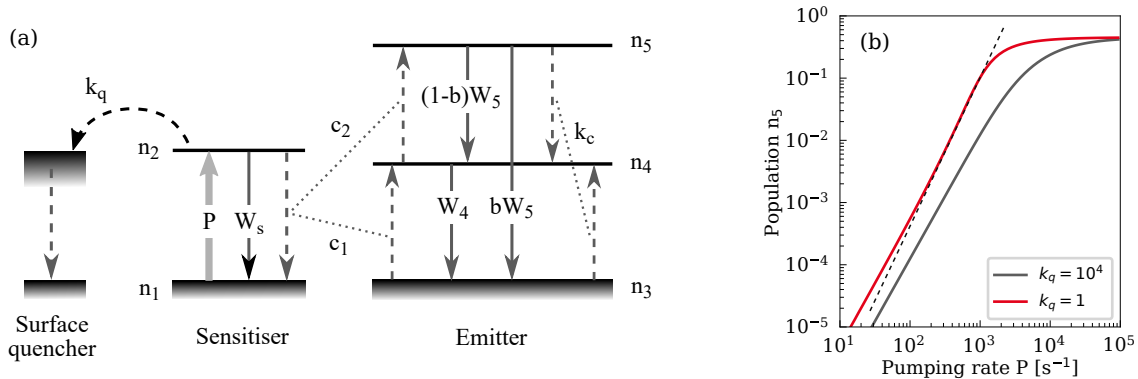
$$n_3 + n_4 + n_5 = 1 \quad (7)$$

where P is the absorption rate of the sensitiser proportional to the excitation intensity, W_s is the intrinsic decay rate of excited sensitiser, $c_{1,2}$ the upconversion coefficients from the sensitiser ion to the emitter ion on its ground and intermediate level respectively, $W_{4,5}$ the intrinsic decay rate of the two excited energy levels of the emitter, b the branching ratio for the emitter decaying from n_5 to n_3 , k_c the cross-relaxation coefficient, k_q the energy transfer coefficient from sensitiser to surface defects.

Table 1: Values of the coefficients for the energy level simulation.

W_s	c_1	c_2	W_4	W_5	b	k_c
10^2	10^4	10^3	10^3	10^3	0.5	10^3

Using the coefficient values in Table 1, we performed the simulation of the excited-state population n_5 of the emitter ion as function of the pumping rate, for two different values of the coefficient k_q representing the energy transfer to the surface defects (Supplementary Figure 10(b)). The population n_5 is directly related to the emission curve as function of the excitation power. When the surface quenching effect is reduced (k_q lowered from 10^4 to 1), the curve slope improves by about 20%.



Supplementary Figure 10: **Numerical simulation of the change in the excitation-emission curve caused by the core-shell structure.** (a) Simplified energy-level diagram of the upconversion process, including a term related to the surface quenching. (b) Population of the highest excited state n_5 directly related to the upconversion emission yield, as function of the pumping rate P . Lowering the coefficient k_q associated with the energy transfer to the surface defects corresponds to the coating of the inert shell around the nanoparticle. Simulations show that reducing the quenching effects significantly improves the emission slope.

Supplementary Note 2: Estimation of the peak intensity

The estimation of the peak intensity was realised by measuring the total beam power delivered to the sample and the transversal beam profile at the focus point. The laser power P_0 was acquired before the microscope objective and the objective transmittance was taken into account. The beam profile was measured by scanning a gold particle with a diameter of 80 nm and by detecting the scattered light intensity at each particle position.

Supplementary Figure 11 shows the transversal profile of the 976-nm excitation laser at the focus point. The beam is characterised by a Gaussian shape, as demonstrated by the best-fit of the experimental data with the intensity profile function $I_{976} = a \cdot \exp(-2r^2/w^2)$ (after performing the subtraction of the background level), where a is the normalisation factor and w the beam waist radius. The best-fit value of the waist radius is $w = 344 \pm 7$ nm, giving a full width at half maximum (FWHM) of 405 nm. Under the assumption of a Gaussian beam, the peak intensity can be evaluate as equal to $2P_0/\pi w^2$.

The 808-nm laser beam originally propagates through a vortex plate which transforms a Gaussian beam into a Laguerre-Gaussian (LG) beam with a topological charge $l = 1$. Therefore, the beam profile would be compatible with a LG intensity profile² at the focus point given by the function:

$$I_{808} = a \cdot (2r^2/\xi^2)^l \cdot \left[L_p^l(2r^2/\xi^2) \right]^2 \cdot \exp(-2r^2/\xi^2) \quad (8)$$

where a is the normalisation factor, $L_p^l(x)$ is the generalized Laguerre polynomial of degree p , and ξ is a profile parameter. In our specific case of $p = 0$ and $l = 1$, the Laguerre polynomial simplifies to the unit constant. Supplementary Figure 12 represents the transversal profile of the 808-nm depletion laser at the focus point. We can characterise our beam profile with the best-fit parameter $\xi = 330 \pm 2$ nm.

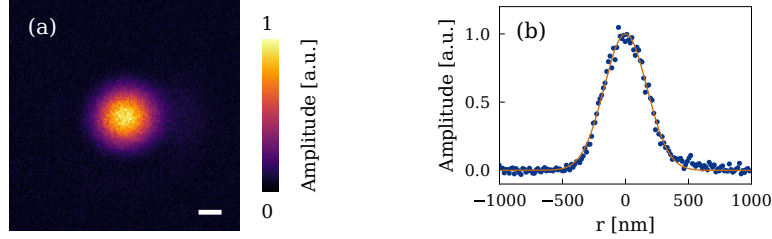
The estimation of the peak intensity for the LG profile is not trivial, and we refer to a more general definition of peak intensity. Given a radial beam distribution $I(r)$ and the relative total power P_0 delivered, we can define the peak intensity at the maximum point p of the beam as the limit of the power enclosed

²R. L. Phillips and L. C. Andrews, "Spot size and divergence for Laguerre Gaussian beams of any order", *Applied Optics* **22**, 643 (1983).

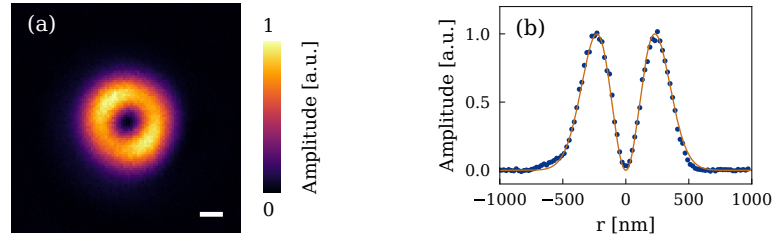
within a small surface S_p surrounding the point p , divided by the same area S_p as the area shrinks:

$$I_p = \lim_{S_p \rightarrow 0} \frac{P_0}{S_p} \int_{S_p} I(r) r dr d\theta \quad (9)$$

If applied to the Gaussian distribution, where the beam peak p is localised at $r = 0$, the equation (9) returns the right value of Gaussian peak intensity, as previously defined. For the annular beam, we first calculate the radius of maximum intensity $r_0 = 233$ nm and then we integrate over the area between the two circumferences $[r_0 - \epsilon, r_0 + \epsilon]$, for $\epsilon \rightarrow 0$. It is important to specify that the normalisation factor a is explicitly calculated as the integral of $I(r)$ over the all radial range $[0, \infty]$.



Supplementary Figure 11: **Experimental beam profile of the excitation 976-nm beam**, used to estimate the power intensity delivered to the sample. (a) Experimental x-y profile of the beam at the focus point. (b) Horizontal line profile obtained at the centre of the beam. The Gaussian fit returns a waist radius of $w = 344 \pm 7$ nm. Scale bar: 200 nm.



Supplementary Figure 12: **Experimental beam profile of the excitation 808-nm beam**, used to estimate the power intensity delivered to the sample. (a) Experimental x-y profile of the beam at the focus point. (b) Horizontal line profile obtained at the centre of the beam. The best-fit of the LG intensity profile as in Equation (8) returns a value for the parameter ξ of 330 ± 2 nm. Scale bar: 200 nm.